ISSN 1069-3513, Izvestiya, Physics of the Solid Earth, 2018, Vol. 54, No. 1, pp. 33–47. © Pleiades Publishing, Ltd., 2018.
Original Russian Text © I.R. Abubakirov, A.A. Gusev, E.M. Guseva, V.M. Pavlov, A.A. Skorkina, 2018, published in Fizika Zemli, 2018, No. 1, pp. 37–51.

Mass Determination of Moment Magnitudes M_w and Establishing the Relationship between M_w and M_L for Moderate and Small Kamchatka Earthquakes

I. R. Abubakirov[a], A. A. Gusev[a,b,c], E. M. Guseva[a,†], V. M. Pavlov[a], and A. A. Skorkina[a,c,*]

[a] *Kamchatka Branch, Geophysical Survey, Russian Academy of Sciences, Petropavlovsk-Kamchatskii, 683006 Russia*
[b] *Institute of Volcanology and Seismology, Far Eastern Branch, Russian Academy of Sciences, Petropavlovsk-Kamchatskii, 683006 Russia*
[c] *Schmidt Institute of Physics of the Earth, Russian Academy of Sciences, Moscow, 123242 Russia*
**e-mail: anna@emsd.ru*

Received June 1, 2017

Abstract—The average relationship is established between the basic magnitude for the Kamchatka regional catalog, M_L, and modern moment magnitude M_w. The latter is firmly tied to the value of the source seismic moment M_0 which has a direct physical meaning. M_L magnitude is not self-reliant but is obtained through the conversion of the traditional Fedotov's S-wave energy class, $K_{S1,2}^{F68}$. Installation of the digital seismographic network in Kamchatka in 2006–2010 permitted mass estimates of M_0 and M_w to be obtained from the regional data. In this paper we outline a number of techniques to estimate M_0 for the Kamchatka earthquakes using the waveforms of regional stations, and then compare the obtained M_w estimates with each other and with M_L, based on several hundred earthquakes that took place in 2010–2014. On the average, for $M_w = 3.0$–6.0, $M_w = M_L - 0.40$; this relationship allows obtaining M_w estimates (proxy-M_w) for a large part of the regional earthquake catalog with $M_L = 3.4$–6.4 ($M_w = 3.0$–6.0).

Keywords: earthquake, magnitude, regional magnitude M_L, seismic moment M_0, moment magnitude M_w, Kamchatka

DOI: 10.1134/S1069351318010019

INTRODUCTION

To solve different problems of seismology, earthquake catalogs are needed that include the estimates of the sizes of the earthquakes expressed on a common magnitude scale. As of now, preference is given to the scale of moment magnitudes M_w (Kanamori, 1977; Hanks, Kanamori, 1979) which is firmly tied to the seismic moment of the source, M_0. In contrast to the traditional magnitudes, which are determined based on the amplitudes at the output of seismic channel, the parameter M_w is qualitatively different and is determined by the conversion from the estimate of a physical parameter, M_0, measured in Newton meters, [N · m]. This conversion is performed by Kanamori's formula (Kanamori, 1977):

$$M_w = (2/3)(\log_{10} M_0\,[\mathrm{N\cdot m}] - 9.1). \qquad (1)$$

We note that in this formula, many authors use the constant −9.05 according to (Hanks and Kanamori, 1979), which contradicts the international standard (Bormann and Dewey, 2014); at the same time, the GCMT service (The Global Centroid-Moment-Tensor Project) since 2006 has used the correct formula. Hereinafter, the development of the methodical basis for unifying the magnitude part of the regional catalog in terms of moment magnitudes is discussed in application to the Kamchatka region.

Moment magnitudes M_w for the recent Kamchatka strong earthquakes are presented in the global GCMT catalog constructed by the technique suggested in (Dziewonski et al., 1981; Ekström et al., 2012), where the lower threshold of magnitude determination for Kamchatka is about $M_w = 4.9$. Besides, a number of independent M_w estimates for the previous strongest earthquakes have been compiled and critically colligated in (Gusev and Shumilina, 2004). However, the moderate and small earthquakes which make up the majority of the past earthquakes remain calibrated on the local magnitude scale M_L—the reference magnitude scale of the Kamchatka and Komandor Islands Earthquake Catalog. This scale is not self-reliant: the M_L values are derived from the values of Fedotov's

† Deceased.

energy class $K_{S1,2}^{F68}$ (Fedotov, 1972) through the conversion by the following formula (Gordeev et al., 2006): $M_L = 0.5K_{S1,2}^{F68} - 0.75$. The $K_{S1,2}^{F68}$ scale (and, thus, M_L) relies on the peak horizontal amplitude A_{peak} of the *S*-wave velocities in the frequency band 0.7–3 Hz: $K_{S1,2}^{F68} = 2\log_{10}A_{\text{peak}} + f(r)$, where r is the hypocentral distance. Hence, the determination of magnitude M_L through $0.5K_{S1,2}^{F68}$ is fairly consistent with the recommended IASPEI terminology (Bormann et al., 2013). To avoid confusion, we note that according to (Fedotov, 1972), on average, $M = \left(K_{S1,2}^{F68} - 4.6\right)/1.5$, where M should be understood as M_S_BB or, equivalently, M_{LH}.

It is instructive to note for clarity that the "energy class" ($K_{S1,2}^{F68}$ or any other) is, in fact, not a logarithm of energy but a kind of magnitude estimate. In principle, the energy of the signal and, based on it, the energy radiated from the source can be estimated by directly integrating the square amplitude of the velocity over time, just as was tried by V.I. Bune (Bune, 1955), who suggested the idea of energy class. However, in the predigital epoch, the mass processing of such kind of data was not possible. The practical alternative which was actually used is to search for and then apply the correlation (statistical but not physical) between the energy estimate and the peak amplitude, as was exercised by T.G. Rautian (1960) and her followers (Fedotov, 1972; etc.). Considering this relationship, Rautian obtained an estimate for the logarithm of energy in the form $K^{P60} = 1.8\log_{10}A_{\text{peak}} + f(r)$. Therefore, in the situation when K^{P60} is used, it is correct to link $K = K^{P60}$ and the local magnitude M_L by the relationship of the form $M_L = K/1.8 + \text{const}$. With the same purpose in the different region, S.A. Fedotov used the formula $K = 2\log_{10}A_{\text{peak}} + f(r)$, so that in the case $K = K_{S1,2}^{F68}$, for the Kamchatka earthquakes, it is reasonable to determine M_L as $K/2 + \text{const}$. Beyond the scope of the correlations, per se, the squared amplitude, $|A(t)|^2$, is always related to the instant signal power $P(t)$, and the integral of $P(t)$ can be conditionally called the "*S*-wave energy":

$$E_S = \int_{t_{Sa}}^{t_{Sa}+T_S} P(t)dt = \int_{t_{Sa}}^{t_{Sa}+T_S} |A(t)|^2 dt, \qquad (2)$$

where t_{Sa} is the arrival time of the *S*-wave and T_S is the duration of the signal from the *S*-wave. At the same time, the peak amplitude which is measured during the determination of M_L or K is related to the peak power rather than with the energy of the signal.

The deployment in 2006–2010 of the network of digital instruments on Kamchatka allowed obtaining variants of the M_w estimates based on the regional network data by applying a number of techniques, which makes it possible to study the relationship between M_L and M_w for moderate and small earthquakes in Kamchatka. With respect to this aim, the following groups of tasks appear: to compare the results of the M_0 and M_w determination in the region by different techniques and to verify the consistence of the obtained estimates; and to reliably establish the average relationship between M_w and the standard regional magnitude M_L for moderate and weak earthquakes. To this end, we obtained the M_0 and M_w estimates by each technique. After this, we compared the results of the different techniques with each other. In order to establish the recommended average relationship between M_w and M_L, we selected a particular M_w estimate for each earthquake by the technique that is preferable for a relevant particular M_w range.

DETERMINING THE SEISMIC MOMENT USING SYNTHETIC SEISMOGRAMS

There are two main approaches to determining seismic moment M_0 from the seismic data. One approach is to estimate the moment tensor components by solving the inverse problem and, to this end, to invert the broadband waveforms with the use of synthetic seismograms, which is described in this section as techniques 1A and 1B, variants of approach 1. Another approach is to use the level of the low-frequency segment of the source displacement spectrum from the body wave data as described in the next section, where 2A, 2B, and 2C denote one of the three techniques—variants of approach 2. When we mean several techniques simultaneously, we will use straightforward designations such as, 1AB or 2BC.

Approach 1, which is based on finding the seismic moment tensor of the centroid (equivalent point source) and has been routinely implemented in the Global Centroid Moment Tensor Project (GCMT), is hereinafter referred to as technique 1A. The project was launched at Harvard University (Dziewonski et al., 1981) and since 2006 the procedures have been passed to Columbia University (Lamont-Doherty Earth Observatory, (Ekström et al., 2012)). Calculations by this technique are published almost in the real-time mode in the global catalog of centroid moment tensor solutions on the project website. These data, hereinafter, denoted by M_w^{GCMT}, were used in the present study. In 1A, the calculations of synthetic seismograms use the global preliminary reference Earth model (PREM) (Dziewonski and Anderson, 1981). We also note that low pass filters with cutoff frequencies 1/40, 1/125 and 1/50 s are used (for the fragments of the record with body waves, mantle surface waves, and crustal surface waves, respectively).

Technique 1B is the embodiment of approach 1 adjusted to the regional data (waveforms from the sta-

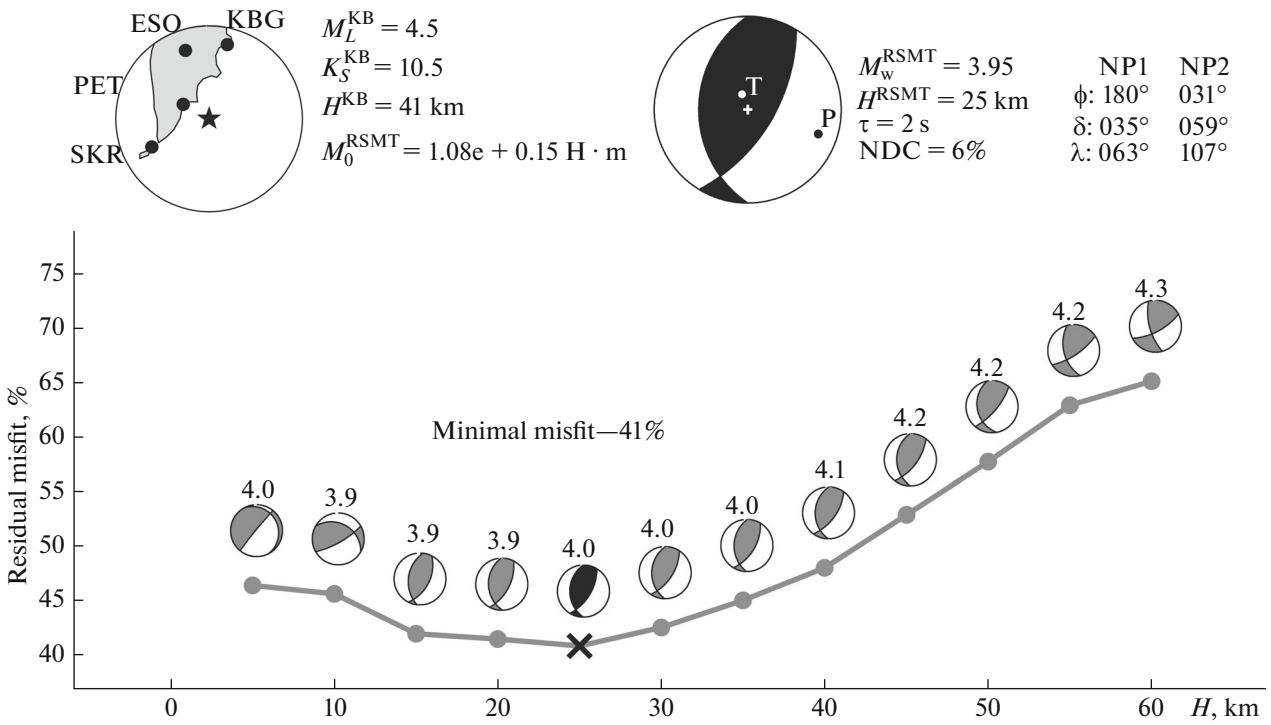

Fig. 1. Depth dependence of residual misfit in inversion of waveforms from earthquake of May 5, 2012, 08:14, $K_{S1,2}^{F68} = 10.5$, $M_w = 3.95$. At each trial depth, stereogram of focal mechanism (lower focal hemisphere) and M_w value are shown. Minimal residual is achieved at depth of 25 km (marked by cross). Shown in upper left corner is location of stations relative to epicenter. Shown in upper right corner is the best mechanism; deviation from "pure" double couple without moment (Non-Double-Couple, NDC) is 6%.

tions of the regional network) and implemented at the Kamchatka Branch of the Geophysical Survey (Pavlov and Abubakirov, 2012) for the Kamchatka earthquakes. The capabilities of the regional digital network deployed in 2006–2010 (Chebrov et al., 2013) in some cases permit seismic moment tensors to be calculated for not only strong earthquakes (as is the case with GCMT, 1A) but also for moderate earthquakes with M_w = 3.6–5.0. In contrast to 1A, synthetic seismograms are calculated in the flat-layered model medium with a relatively small number of layers. The parameter values for the medium were derived from the global model of the Earth ak135 (Kennett et al., 1995). Another significant distinction of technique 1B from 1A lies in the use of filters that are different from 1A; periods of 15–50 s are used, and the complete waveform is analyzed rather than its fragments (Figs. 1 and 2). The results of calculations by technique 1B are denoted by M_w^{RSMT}, where RSMT is the regional estimate of the seismic moment tensor of the equivalent point source.

The preprocessing of seismograms for inversion by technique 1B includes reconstructing the true ground displacements—deconvolution (in time domain) and calculation of the radial and transverse components. The position of the epicenter is fixed based on the catalog data. Next, the optimal variant is determined by fitting for two parameters: the depth and source duration. The necessity of fitting the source duration is associated with the fact that in the analysis of strong earthquakes, the finite duration of the source time function significantly affects the time histories of synthetic seismograms. The duration for small earthquakes is not varied but assumed to be 2 s. With the fixed depth and duration, the inversion of the selected segments of the ground motion broadband seismograms is carried out with the use of synthetic seismograms (Pavlov, 2013), i.e. the responses of the medium to the elementary sources corresponding to the particular components of seismic moment tensor (SMT). Before the inversion, both the real and synthetic ground motion records are processed by the fourth order bandpass Butterworth filter. The band pass period of the filter is either 16 to 25 or 20 to 50 s, depending on which of these intervals the signal-to-noise ratio is higher; generally, the lower frequency pass band is preferred. The optimal variant is selected by the value of the minimum generalized residual which points to the closest agreement between the real and synthetic ground displacements. The described technique is implemented in the interactive mode. The result of this processing is tensor $M_{ij} = M_0\, m_{ij}$, where M_0 is the sought scalar seismic moment and the unit tensor m_{ij} specifies the focal mechanism. The

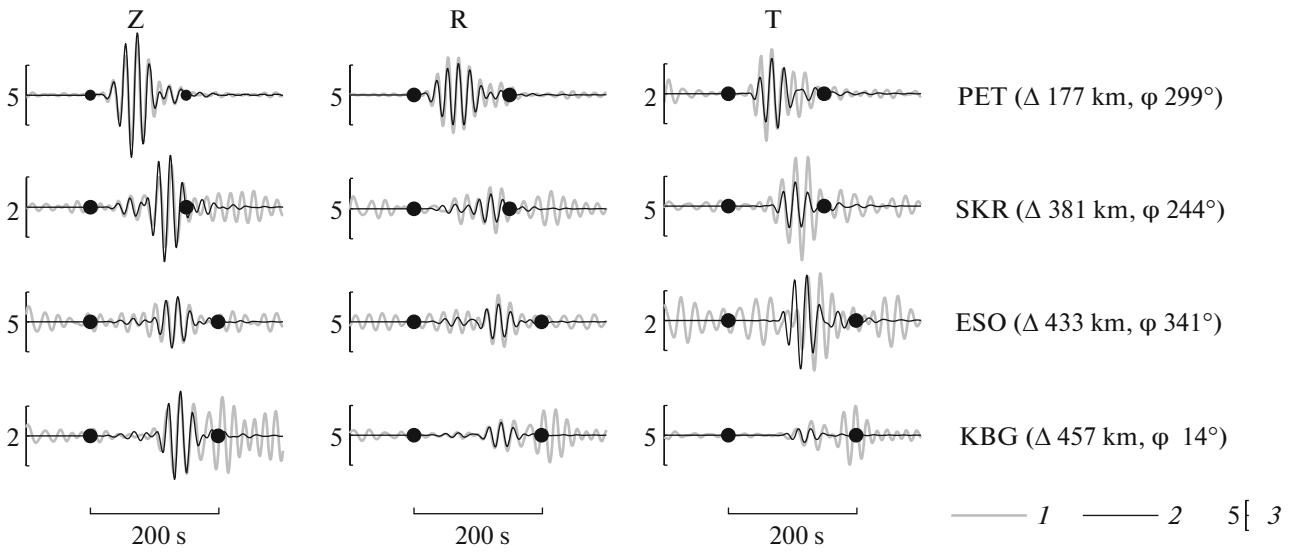

Fig. 2. Comparison of real (*1*) and synthetic (*2*) ground displacement waveforms for optimal depth (25 km) for earthquake of May 6, 2012 at 08:14, $K_{Sl,2}^{F68} = 10.5$, $M_w = 3.95$. Amplitude scale (*3*) is indicated in units of 10^{-5} cm. Dots show ends of fitting interval. Filtering pass band is 16–25 s. Limited agreement between synthetic and real seismograms (filtered) indicates significant inconsistency between assumed horizontally layered model and real 3D heterogeneous medium.

obtained M_0 value is further converted into M_w by formula (1).

The techniques of the first approach (1A and 1B) provide a reliable estimate of M_0 and M_w; however, they are not free from important limitations. Among the latter the key one consists in the impossibility of obtaining stable estimates of M_0 and M_w for the relatively smaller earthquakes, which is due to the signal-to-noise ratio degradation at low frequencies under the reduction of magnitude. In fact, in technique 1A, the lower threshold of M_w^{GCMT} determination is $M_w \approx 4.9$ (Fig. 5a), whereas in technique 1B, a similar threshold for M_w^{RSMT} is $M_w \approx 3.6$ (Figs. 5b–5d).

DETERMINING THE SEISMIC MOMENT USING THE SPECTRA OF RECORDS

The refinement of the regional attenuation model (Gusev and Guseva, 2016) and mass determination of the source spectra for the Kamchatka earthquakes (Skorkina and Gusev, 2017), including the source spectra of ground displacements made it possible to apply the second approach. The key advantage of approach 2 lies in the possibility of putting down the threshold of determination of M_w in the catalog. This fairly traditional approach (Brune, 1970; Aptekman et al., 1989; Guseva et al., 1991) uses a simplistic theoretical model: the amplitudes are determined based on ray seismics; the spectral levels on the different rays are averaged, and the calculations use the focal-sphere-averaged radiation pattern for the squared amplitudes of the *S*-waves. Within the spectral approach, we tested three techniques which differ by the spectrum calculation scheme and/or time window for calculating the spectrum (Fig. 3). The first one, technique 2A, uses the spectrum for the group of *S*-waves calculated through the discrete Fourier transform (DFT). We denote these estimates by M_w^{SF} where *F* stands for Fourier. The spectral calculations in technique 2B employ multiple bandpass filtering of the *S*-wave group. The resulting estimates are denoted by M_w^{SB}, where *B* stands for Band. We note that the difference between techniques 2A and 2B is largely technical: for the ideal conditions, the theory (Parseval equality) guarantees the identity of the spectra of the records calculated by the Fourier transform and by the analysis of the output signals of the bandpass filter bank. In both techniques (2A and 2B) the spectrum of the *S*-wave record is converted into the source spectrum with allowance for losses and other factors. An important advantage of technique 2B, compared to 2A, is that it allows automating the process. In technique 2C, which largely relies on the approach of T.G. Rautian and V.I. Khalturin (Rautian and Khalturin, 1978), estimation of the source spectrum is based on the power spectrum of the coda waves at a fixed lapse time from the time of origin. Techniques 2BC use a two-stage loss account procedure. Initially, the spectrum of a *S*-wave or coda is converted into an *S*-wave spectrum at a fixed distance $r_{tr} = 50$ km; to this end, the preliminarily calculated empirical attenuation functions are used in each band. Next, from $r_{tr} = 50$ km to $r_0 = 1$ km, the obtained estimate for the *S*-wave spectra is converted into the source spectrum taking into account

the assumed models of geometrical spreading and losses. An important element of the 2ABC techniques is the use of empirical spectral station corrections, which allow the obtained station spectra to be reduced to the reference hard-rock station conditions. The station corrections are found by determining the average (over the entire set of earthquakes) ratios of the *S*- and coda-wave spectra of each station to the *S*- and coda-wave spectra at the reference station for the same earthquake. The procedure for determining the station corrections is described in detail in (Skorkina and Gusev, 2017). As a reference station, the PET hard-rock station is assumed. Arguments in favor of this selection are presented in (Gusev and Guseva, 2016; Pavlenko, 2013). Both the 2BC techniques are implemented in the automated mode. In all the three 2ABC techniques, individual estimates of a flat spectral level were obtained from each station, whereas the network-mean estimates for each technique were determined by averaging. Let us consider the variants of the 2ABC approach in greater detail.

In the *2A technique*, the seismic moment estimate M_0 is derived from the level of a flat segment of the source spectrum converted from the ground displacement spectrum of the body *S*-wave (technically, the latter is calculated through DFT). The time window of the group of direct *S*-waves in the earthquake record is selected interactively within the interval with a width of 10–30% of the *S*-wave travel time. The selected segment is multiplied by half of the cosine window within the terminal 5% of the segment duration and then subjected to DFT. After this the amplitude spectrum is smoothed within the 2/3 octave pass band; a fixed step of 0.05 by the log frequency is used.

Next, the observed spectra are converted to the source spectra. In the 2A technique, the spectra are corrected for the geometric spreading of the body *S*-waves which is assumed to be spherical (by $1/r$, where r is the hypocentral distance). (In the 2B technique, a more accurate two-stage procedure is used for the same purpose: the spectra are initially reduced to $r_{tr} = 50$ km using the preliminarily determined empirical attenuation functions (calibration curves), and only after this step, the processing follows technique 2A.) Ray bending is disregarded. After this, the corrections are introduced for the losses along the ray path (using the $Q_S(f)$ estimates from (Gusev and Guseva, 2016), for the impedance difference between the case of a station recording on the surface of a layered crust and the case of an elastic half-space. The procedure for determination of impedance correction which follows the technique of (Boore, 2003) is described in (Skorkina and Gusev, 2017). This impedance correction emerges within the ray method for the medium, including the layered one, with smoothly varying velocities. This way, the spectra are reduced to the standard small hypocentral distance $r_0 = 1$ km and the case of a uniform half-space.

Next, the seismic moment M_0 (N m) is estimated by the formula (Bormann et al., 2013)

$$M_0 = \frac{\Omega_0 4\pi\rho r_0 v_S^3}{0.63 \times 2.0}, \quad (3)$$

where Ω_0 is the level of the flat spectral segment of the total *S*-wave displacement vector (m · s) reduced to the conditions of an elastic uniform half-space; ρ is the density of the medium (kg/m^3); r_0 is the standard distance (1000 m); v_S is the velocity of *S*-waves (m/s); 0.63 is the focal-sphere root mean square radiation pattern for the *S*-wave total vector (Boore and Boatwright, 1984); and 2.0 is coefficient that accounts for the free surface effect. The use of the average radiation pattern is common for the spectral method; it is due to this simplification that for each earthquake we can simply average the estimates over the stations. The value of Ω_0 is determined from the sum of the squared component spectra. In the conditions of low-accurate source depth estimates and structural complexity of the medium, it is frequently unclear whether a particular source is located above or below the Moho. However, the results for the Kurile zone (east of Hokkaido Island), which were obtained with the use of ocean bottom seismometer stations (Mayeda and Sasatani, 2006), suggest that most of the sources are located in the mantle. In this situation, with limited reliability, the mantle parameters are assumed to be (Guseva et al., 1991) $\rho = \rho_{(source)} = 3300$ kg/m^3 and $v_S = v_{S(source)} = 4700$ m/s.

Technique 2B does not fundamentally differ from 2A; it also uses the level of the flat segment of the source displacement spectrum; however, it is implemented in a technically different way: the spectrum of the record is determined by band pass filtering. The band pass filter set is used, each filter with a 2/3 octave (0.2 decade) pass band, with center frequencies 0.25, 0.4, 0.63, ..., 25, 40 Hz (step 0.2 in $\log_{10} f$). After bandpass filtering, for each band the integral of squared amplitude is calculated and summed over three components. The result "energy of the signal" corresponds to Eq. (2) with $A(t)$ understood as the output signal of bandpass filtering. (Throughout the paper, "energy" in quotation marks is used as an analog of "power" in the power spectrum; however, multiplication of the bandpass filter output (analog of (2)) by ρc_S^2 would yield the *S*-wave energy flux density in the band [W/m^2].) In 2B, the segment of the record (time window) used for the integration is expanded. This window starts at the time of the *S*-wave arrives and has a width of 0.8 t_S, where t_S is the *S*-wave travel time. Hence, the window length is proportional to the traveltime t_S. We can substantiate this choice, by referring to (Petukhin and Gusev, 2003), where it is shown that in the conditions of Kamchatka, for moderate earthquakes, due to the effects of scattering, the wave train of the *S*-waves expands over the time period proportional to the travel time.

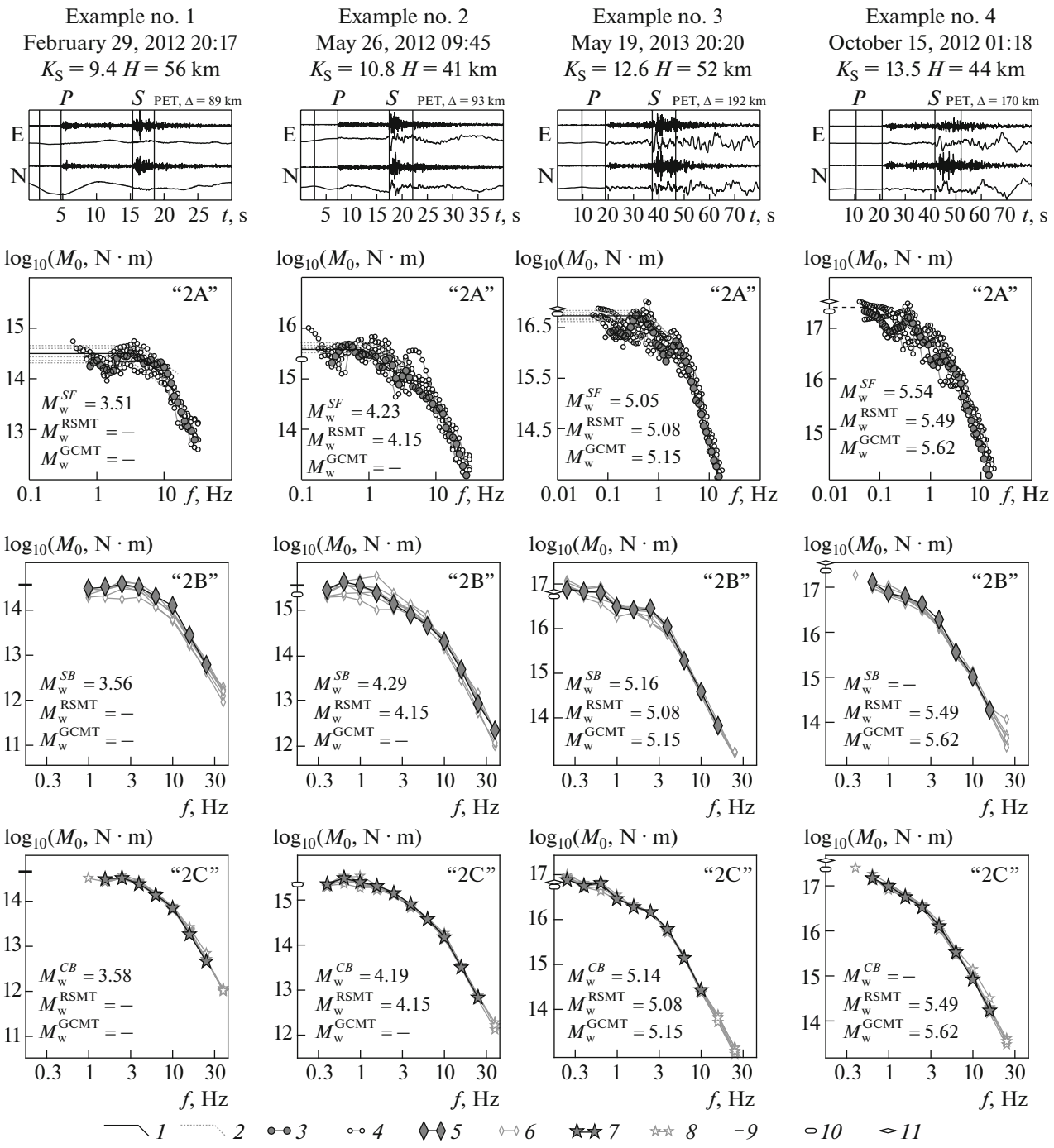

Fig. 3. Illustration of spectral techniques for determining M_0. Examples for four earthquakes are presented columnwise. Parameters and magnitude (class) of events are indicated in header. Shown from top to bottom: first line: record of acceleration and displacement in *E*- and *N*-components; second line: source *S*-spectra (technique 2A); third line: source *S*-spectra (technique 2B); fourth line: source *S*-spectra (technique 2B). In 2A: (*1*) are polylines approximating observed spectra at PET station to model displacement spectra; kink point of these polylines fixes the selection of corner frequency f_c; (*2*) same for other stations; (*3*) *S*-spectra from PET station; (*4*) *S*-spectra from other stations. In 2B: (*5*) network-average *S*-spectrum; (*6*) individual *S*-spectra for each station whose averaging yielded network-average *S*-spectrum (*5*). In 2C: (*7*) network-average *CS*-spectrum; (*8*) individual *CS*-spectra for each station whose averaging yielded network-average *CS*-spectrum (*7*). In 2B and 2C: (*9*) automatically picked levels for network-average spectra. In 2A, 2B, 2C: (*10, 11*) levels corresponding to $\log_{10} M_0^{\mathrm{RSMT}}$ and $\log_{10} M_0^{\mathrm{GCMT}}$, respectively. In example 4 of 2B and 2C, segment has not been identified as reliably flat; and therefore, level has not been picked automatically; however, it was selected interactively in procedure 2A.

Next, for each band, the acceptability of the estimate is checked from the standpoint of the signal-to-noise ratio. The noise level was determined within at least a 60-s window before the *P*-wave's arrival. The threshold signal-to-noise amplitude ratio was assumed to be 2. The estimates from the noised bands are rejected. Under the assumption of smoothness of the spectral source function, the "signal energy" in each band is converted to the level of the Fourier amplitude spectrum in the same band by Parseval's equality; the set of bands gives the averaged amplitude spectrum. The further conversion of the observed spectrum into the source spectrum follows the procedure described above in relation to technique 2A. The spectral levels are converted into the seismic moment M_0 by formula (3).

In *technique 2C*, the estimate of the seismic moment M_0 is determined from the flat level of the *S*-wave power spectrum determined from coda power. The last level is determined by bandpass filtering at a certain lapse time from the origin time and then reduced to a fixed time delay of 100 s. To this, the instantaneous coda power is estimated within the limits of an appropriate time window ($[t_1\ t_2]$) and then reduced to 100 s using the standard regional temporal decay function of the coda amplitudes for a given band. In this way, the root mean square coda level $\log_{10} A_{C100}(f)$ is determined in each band. The band set is the same as in technique 2B. The minimal acceptable length of the time window $[t_1\ t_2]$ for estimating the coda level is 6 s. The value of t_1 is specified by $L_1 \times t_S$ where, following (Rautian et al., 1981), L_1 is assumed to be frequency-dependent, from $L_1(f) = 2.3$ for 0.25 Hz to $L_1(f) = 1.7$ for 40 Hz. The selection of t_2 is determined by the noise level. In case of possible aftershocks contaminating the coda, the time window is shortened (or even the data are totally rejected). Cutting off the aftershock record is conducted by an efficient automated algorithm. The first variant of the standard empirical regional coda envelopes for a set of frequency bands was determined in (Abubakirov and Gusev, 1990) from the photo records by the frequency selective seismic stations (ChISS). In the present work, we use refined curves which were recently estimated over a large set of digital records (Chebrov and Gusev, to be submitted). Then, the power spectrum $\log_{10} A_{C100}(f)$ is converted to the *S*-wave amplitude spectrum at $r = r_{tr} = 50$ km. To ensure this possibility, the mentioned empirical calibration curves for the *S*-waves during their construction are tied to $\log_{10} A_{C100}$—the coda level at 100 s. Then just as in techniques 2A and 2B, an estimate of the flat level of the source displacement spectrum is taken; the low frequency (LF) spectra levels are converted into the seismic moment M_0 by formula (3).

For estimating M_0 and M_w in technique 2A, when possible, a flat low-frequency segment is selected in the obtained source spectrum. This is done interactively for the data of each station after which the station estimates of $\log_{10} M_0$ and M_w are averaged (Fig. 3). In the automated 2BC techniques, the station estimates of the source spectra are initially averaged over the set of stations and then the network-average source spectrum is analyzed from which spectrum the network-average $\log_{10} M_0$ and M_w estimates are determined when low-frequency flat segment can be identified. It was possible to obtain these network-average estimates in 86, 57, and 61% of the cases by techniques 2A (M_w^{SF}), 2B (M_w^{SB}), and 2C (M_w^{CB}), respectively, for 890, 589, and 636 earthquakes (Figs. 4b, 4d, 4c). Hence, on average, the automated procedure (2BC) qualifies the segment in the LF part of the source displacement spectrum as reliable only in two of three cases, and its level is picked only in these cases. These variants are illustrated in Fig. 3, where there are cases of the approximately flat reconstructed displacement spectrum (examples nos. 1–3), which are acceptable for obtaining the M_0 estimate; there is also the alternative case where no reliable flat segment can be seen (example no. 4). In most of these cases, the fact that M_0 cannot be reliably determined from the *S*-waves is in fact related to the unacceptably low signal-to-noise ratio at low frequencies.

INITIAL DATA

The initial data for M_L are available from the regional catalog (*Kamchatskii...*, 2017). The M_w estimates were obtained by the two described approaches of data analysis: approach 1 (techniques 1A, 1B) and approach 2 (techniques 2A, 2B, 2C). In technique 1A, since 1988, the Global Seismic Network (GSN) data have been used. This network includes more than 150 stations, with the international network codes II (the network operated by the Incorporated Research Institutions for Seismology, IRIS) and IU (a joint network of IRIS and the United States Geological Survey (USGS)). The remaining techniques (1B, 2A, 2B, 2C) rely on regional data, specifically, the waveforms from the Kamchatka digital seismic station network of code D0 (in the database of the International Federation of Digital Seismograph Networks).

For each approach (1B, 2ABC), considering the capabilities of the techniques, we compiled two collections of earthquake records, which considerably overlap in the sense of the sets of events. The collections differ by the number of the earthquakes and/or lower magnitude threshold (Table 1), as well as by the set of stations. We also note that velocity records are used for technique 1B and accelerograms are used for techniques 2ABC.

The set of data used for technique 1B (referred to as the first collection) includes the events of 2011–2012 mainly from the region between 50.0° and 56.0° N and between 157.0° to 162.0° E with $K_{S1,2}^{F68} = 9.0$–13.0 (Fig. 4a).

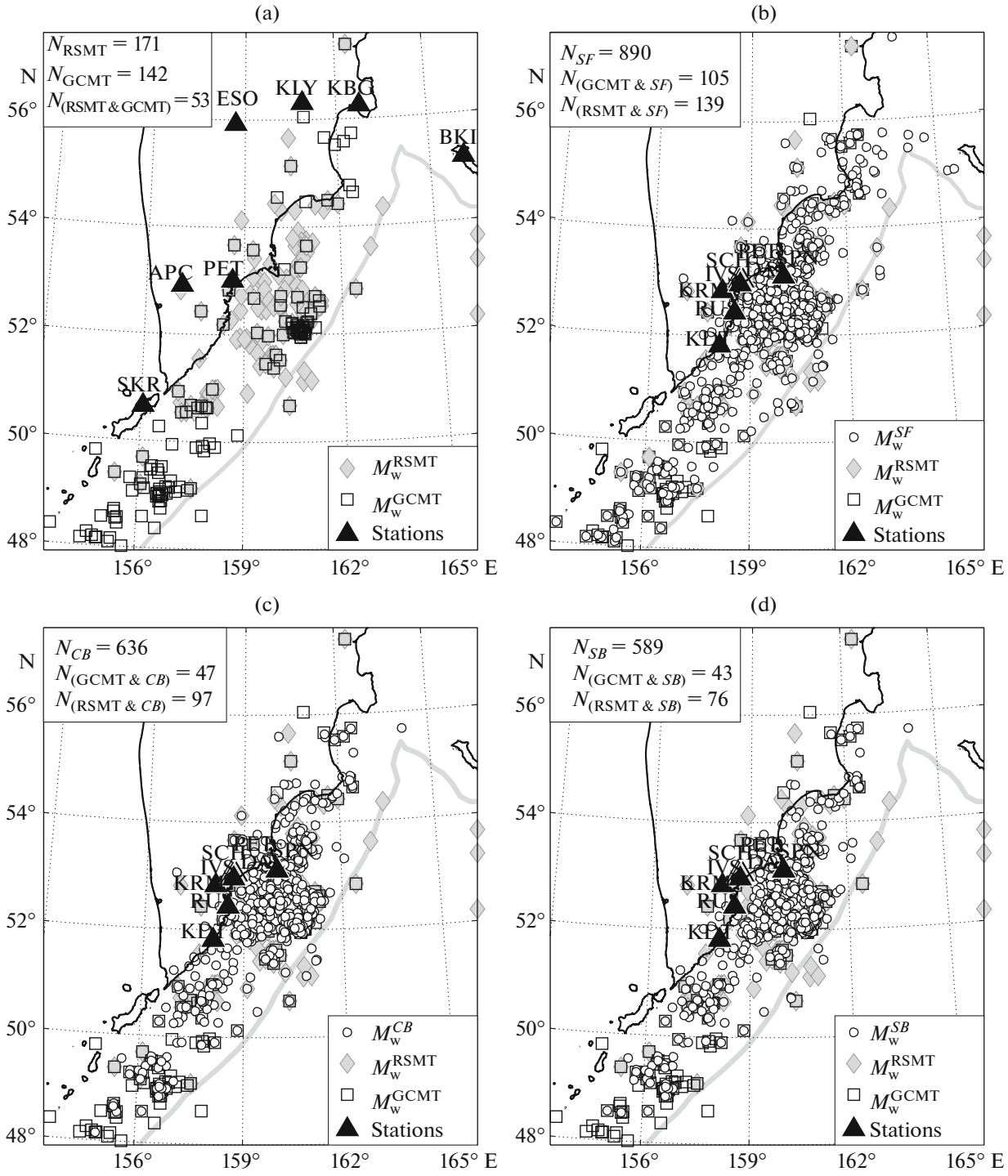

Fig. 4. Epicenters of earthquakes for which estimate was obtained (a) by 1B—M_w^{RSMT}; (b), 2A—M_w^{SF}; (c) 2C—M_w^{CB}; (d) 2B—M_w^{SB}. Positions of seismic stations involved in analysis are marked.

Besides, this collection also includes the Zhupanovskoe earthquake of January 30, 2016 with M_w = 7.2 (Chebrov et al., 2016) and the Toludskoe earthquake of November 30, 2012 with $K_{S1,2}^{F68} = 11.3$ close to the Tolbachik volcano. All the broadband seismograms (from the velocimeters at stations PET, APC, KBG, BKI, SKR, KLY and ESO) prepared for the inversion are characterized by a fairly high signal-to-noise ratio and are free of clipping (ADC overflow). With these constraints, processing by the first approach (1B) was only possible for the records of 171 earthquakes of the first collection.

Table 1. Comparison of data sets for M_w determination

	Technique of M_w determination				
	M_w^{GCMT}	M_w^{RSMT}	M_w^{CB}	M_w^{SB}	M_w^{SF}
M_w range studied	4.8–6.8	3.6–6.6	2.7–6.1	2.7–5.7	2.6–6.4
Number of stations involved	8–159	3–5	3–8	3–8	3–8
Number of earthquakes studied	142	171	636	589	425
Approximate lower threshold of catalog completeness M_w	4.9	3.9	3.2	3.2	2.9

Interstation scatter of M_w^{SF} is determined from estimates obtained by averaging over at least three stations, namely, 425 estimates of obtained 890; i.e., 465 M_w^{SF} estimates are obtained by averaging over two stations.

For approaches 2ABC, we used another set of earthquakes—the second collection, which includes events with $K_{S1,2}^{F68} = 7.0–15.2$ over the period from 2010 to 2014 in the region 48.0°–57.5° N, 153.5°–165.5° E with source depths less than 200 km. Here, records from eight hard-rock or semi-hard-rock stations are used (Figs. 4b–4d): PET (Petropavlovsk), DAL (Dal'nii), IVS (Institut), KDT (Khodutka), KRM (Karymshina), RUS (Russkaya), SCH (Shkola), and SPN (Shipunskii). When compiling the second collection, we have excluded, under visual inspection, the records of earthquakes that were not preceded by at least a 2-min interval of microseismic noise (e.g., those containing the record of the previous earthquake, a typical situation in the case of an earthquake swarm) and the records of "multiple" earthquakes (with at least three clear arrivals of groups of body waves). At the next stage, we also rejected the waveforms whose spectra either have a complicated shape (a sufficiently distinct flat segment in the displacement spectrum is absent, or spectral bumps that are not specific of a particular station are observed) or a signal-to-noise ratio below 2 in the 0.7–10 Hz band, which is amply covered in most of the studied records. In accordance with the described criteria, about two-thirds of the total of 6328 records of 1111 earthquakes were found suitable for processing by the second approaches (2ABC). These 4326 records of 1034 earthquakes from eight stations compose the second collection.

CROSSCOMPARISON OF DIFFERENT M_w ESTIMATES IN THE REGION

Statistics of the differences of estimates. The overall numerical characteristics of the results obtained by the described techniques are summarized in Tables 1, 2. The main one, Table 2, presents the results of pair comparisons (except for the cells with semibold numbers). These are the triples of $\mu/\sigma/N$, where μ is the mean, σ is the standard deviation of the difference $M_1 - M_2$ of two network-average estimates for two techniques, where M_1 is the magnitude indicated in the table's heading; M_2 is the magnitude in the first column; and N is the number of pairs of estimates used. The diagonal cells of Table 2 (shown in semibold) present the data for individual techniques. These are the triples $\mu'/\sigma'/N'$, where $\mu' \equiv 0$ is the mean and σ' is an estimate of the rms accuracy of the station estimates of M. In the conditions of unknown true M, this estimate is determined by formula $\sigma' = \left(n/(n-1)\right)^{0.5} \sigma_1$, where n is the number of stations and σ_1 is the rms value of the intranetwork residual. In other words, σ_1 is the average over rms differences $M_{st} - \overline{M}$, where M_{st} is the station estimate of M and the horizontal bar denotes network averaging. A comparison of the estimates by different techniques is illustrated in Fig. 5.

Studying the consistency of estimates. In Table 2 it is shown that the low-frequency estimates, namely, M_w^{RSMT} (regional) and M_w^{GCMT} (global), closely agree with each other, which testifies to their reasonably high accuracy. For instance, for 53 RSMT–GCMT intersections, $\mu = -0.09$ and $\sigma = 0.08$ (Table 2, Fig. 5a).

For verifying the M_w^{CB}, M_w^{SB}, and M_w^{SF} estimates, they are compared to M_w^{GCMT} and M_w^{RSMT}. These two estimates are assumed to be the reference estimates due to the following considerations. Firstly, the period range used in the calculations of M_w^{RSMT} is at least 20–30 s and longer, which better agrees with the definition of M_0 as the limit of the source spectrum with the frequency tending to zero. Secondly, the theoretical model used in the calculations of M_w^{GCMT} and M_w^{RSMT} is more adequate in the work frequency range (required for determining M_0) than the model used in approaches 2ABC. For estimates based on the spectra of the *S*- and coda waves, the agreement with the LF estimates is somewhat worse than between these estimates; however, we still consider it admissible.

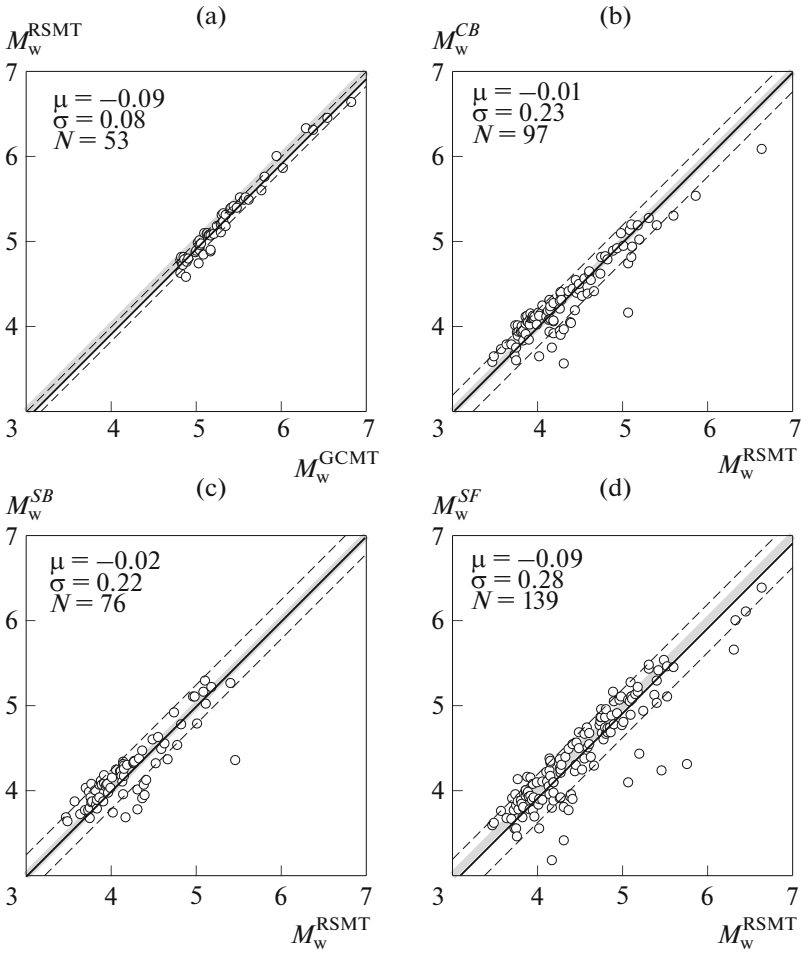

Fig. 5. Relationships between magnitudes M_w^* and M_w^{LF}. Abscissa axes shows (a) M_w^{GCMT}; (b), (c), (d) M_w^{RSMT}. Ordinates of graphs are (a) M_w^{RSMT}; (b) M_w^{CB}; (c) M_w^{SB}; (d) M_w^{SF}. Average relationship is given by solid line $y = x + \text{const}$, where const = μ, dashed-dotted lines are graphs with const = μ ± σ, where σ is standard deviation. Solid gray lines correspond to 1 : 1 type of relationship (when $M_w^* = M_w^{LF}$). Shown in left upper corners are values of μ, σ, *N* obtained by data approximation by linear orthogonal regression with fixed $b = 1.0$.

The reduction of the lower threshold of M_w, which is achieved by each of the regional techniques (1B and 2ABC, Table 1), is an important result.

RELATIONSHIP BETWEEN REGIONAL MAGNITUDE M_L AND M_w

It is of considerable practical interest to compare the M_w estimates with the local magnitude $M_L(K_{S1,2}^{F68})$. The theory and many empirical studies lead us to expect, firstly, that this relationship is likely to be nonlinear and, secondly, in the case of linearity or weak nonlinearity, the slope (*b*-value) of the obtained linear relationship is likely to differ from 1.0. However, against expectations, it turned out that the both these assumptions were not fulfilled. Firstly, the assumption of a linear relationship between M_L and M_w in the studied interval M_w = 3.0–6.0 (M_L = 3.4–6.4) is acceptable. Secondly, the *b*-value of the observed linear relationship is close to 1.0 or, which is the same, the difference of these magnitudes is close to constant. The results are shown in Fig. 6 and Table 3. The recommended relationships (Fig. 7) only for the range M_w = 3.0–6.0 or M_L = 3.4–6.4 are

$$M_w = M_L - 0.40, \quad (4)$$

$$M_w = 0.5(K_{S1,2}^{F68}) - 1.15. \quad (5)$$

DISCUSSION

The M_w estimates obtained from the body *S*-waves (M_w^S) and coda waves (M_w^C) at frequencies ~0.3–3.0 Hz should ideally coincide with the independent estimates, e.g., based on the surface wave data (for instance, M_w^{GCMT}) or other LF data (M_w^{LF}). Actually,

Table 2. Cross characteristics and internal characteristics of M_w determination accuracy

	M_w^{RSMT}	M_w^{CB}	M_w^{SB}	M_w^{SF}
M_w^{GCMT}	−0.09/0.08/53	−0.23/0.18/47	−0.23/0.21/43	−0.25/0.24/105
M_w^{RSMT}	—	−0.01/0.23/97	−0.02/0.22/76	−0.09/0.28/139
M_w^{CB}		**0/0.08/636**	−0.01/0.07/496	−0.08/0.15/592
M_w^{SB}			**0/0.18/589**	−0.09/0.12/542
M_w^{SF}				**0/0.09/425**

Triplet of numbers in cell is (mean difference, μ/standard deviation, σ/sample volume, *N*); σ in bold-faced cells characterizes individual technique; σ in other cells characterizes scatter of difference between pair of techniques. All differences are calculated by scheme heading minus first column. Other details are in text.

our M_w estimates are somewhat lower. Similar small systematic deviations were also observed in other regions (Table 4). This table presents the values of $dM_w = M_w^{S(C)} - M_w^{LF}$, where $M_w^{S(C)}$ is the estimate by the local *S*- or coda waves and M_w^{LF} is the estimate based on the LF signals (M_w^{GCMT} and M_w^{RSMT}). There are also cases (e.g., (Edwards et al., 2010)) when the authors formulate the results of the work as the

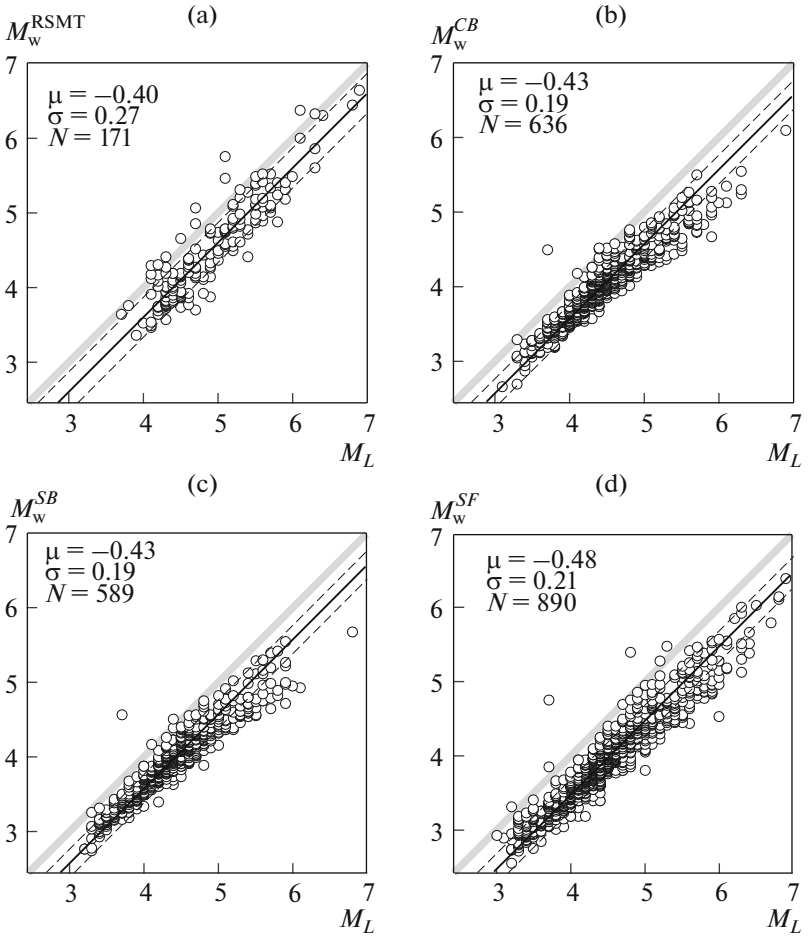

Fig. 6. Relationships between magnitudes M_w and M_L. Abscissa is everywhere M_L, ordinates are (a) M_w^{RSMT}; (b) M_w^{CB}; (c) M_w^{SB}; (d) M_w^{SF}. Average relationship is given by solid line $y = x + \text{const}$, where const = μ, dashed-dotted lines are graphs μ ± σ, where σ is standard deviation. Solid gray lines correspond to 1 : 1 type of relationship (when $M_w^* = M_L$). Shown in left upper corners are values μ, σ, *N* obtained by data approximation by linear orthogonal regression with fixed $b = 1.0$.

Table 3. Relationship of M_w estimates obtained by different techniques with regional magnitude scale $M_L(K_{S1,2}^{F68})$

Technique of M_w determination	N pair	$\mu(M_w-M_L)$	$\sigma(M_w)$	$\sigma(M_w-M_L)$
M_w^{GCMT}	142	−0.33	–	0.25
M_w^{RSMT}	171	−0.40	–	0.27
M_w^{CB}	636	−0.43	0.08	0.19
M_w^{SB}	589	−0.43	0.18	0.19
M_w^{SF}	890	−0.48	0.09	0.21

$\sigma(M_w)$ is accuracy of network-average M_w estimated from inter-station scatter of estimates; $\sigma(M_w-M_L)$ is standard deviation of individual residuals M_w-M_L.

absence of perceivable discrepancies between $M_w^{S(C)}$ and M_w^{LF}; however, the step of calculating M_0 at which the correction for the difference in impedances is introduced, is skipped; in other words, the model of a uniform half-space is used. If the impedance correction were introduced, a discernible discrepancy dM_w would have been found.

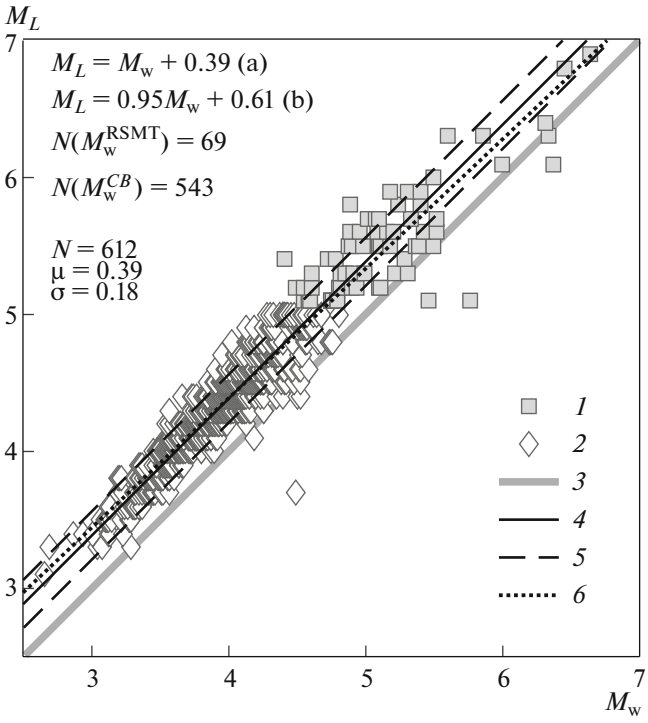

Fig. 7. Dependence of M_L on M_w, where M_w is selected in following way: for $M_L > 5$ it is M_w^{RSMT} (*1*), for $M_L \le 5$, it is M_w^{CB} (*2*). Line *3* is drawn with $M_w = M_L$ assumed. Under assumption of linear relationship with $b = 1$, average relationship ((*4*) Eq. (a)) and its $\pm\sigma$-interval are shown (*5*). Also, data approximation by linear orthogonal regression without fixing b-value is presented ((*6*) Eq. (b)).

It is also worth noting that, although the use of the LF data should, in principle, yield more stable M_0 (and M_w) estimates than those based on *S*-waves, a special study (Gasperini et al., 2012) demonstrated the opposite. It was established that the systematic deviations reaching 0.2 log units exist between the LF-based estimates determined by different technologies. Discrepancies of this kind are typically passed over in silence or attributed to differences in the models of the medium assumed in the calculations by the two methods. However, there are also alternative possibilities discussed below. Overall, considering the international experience, we believe that the systematic deviations of $M_w^{S(C)}$ from M_w^{RSMT} (and of $M_w^{S(C)}$ from M_w^{GCMT}) are rather small and the spectra-based estimates (the 2ABC approaches) can be treated to be entirely acceptable in the studied range of magnitudes.

In the case discussed, with allowance for the data of Table 2, the deviation $M_w^{RSMT}-M_w^{GCMT} \approx -0.05...-0.15$ should be considered as statistically significant. Here, it can be believed that the M_w^{RSMT} estimates better represent the reality due to certain advantages. Specifically, their depth estimates are probably more accurate; besides, the source durations in the cases when they were not short were fitted individually. The estimates based on the *S*- and coda waves are reasonably close to M_w^{RSMT} but may contain, on average, a downward bias by about −0.1 log units (e.g., see the discrepancy between the M_w^{CB} and M_w^{SB} estimates in Table 2). This discrepancy may reflect some methodical drawbacks of the spectral approach. However, in the case of stronger earthquakes (M_w = 5–6), the relatively small negative bias of the estimates based on the S-waves compared to the LF estimates may reflect physical factors.

The source spectrum in the frequency band 0.5–0.02 Hz (period 2–50 s) is not necessarily strictly constant but may increase slightly at lower frequencies due to the contribution of the slow postseismic creep or the afterslip. For a part of the obtained spectra, the segment at low frequencies is not entirely flat but, rather, gently oblique (earthquake no. 4 in Fig. 3 is an example) with a slow spectral decay with the increase in frequency. In these cases, the M_w estimate based on the lower frequency data (e.g., surface waves) will always be higher than the medium-frequency estimate (e.g., based on the spectrum of *S*-waves). This situation can be suspected in the basis of the fact that all the discrepancies of this type—in our case and in all the cited examples—have the same (negative) sign, as should be expected if our explanation is valid. It is not unlikely

that even the small discrepancy between M_w^{GCMT} and M_w^{RSMT} has the same nature.

A similar trend is also known of the M_w^{GCMT} estimates; i.e, at $M_w \sim 9$ the M_w^{GCMT} estimates may have some negative bias which becomes apparent when a lower frequency M_w estimate based on the amplitudes of the free oscillations of the Earth with periods of 1000–2000 s is available. This problem arises when the longest periods involved in the inversion are shorter than the duration of the source (Tsai et al., 2005). For example, for the source of the offshore Sumatra earthquake of 2004 (Indonesia), the upper limit duration of the source time function was estimated at 300–600 s, while the inversion was performed in the interval of periods from 300 to 500 s, which eventually resulted in the estimate $M_w^{GCMT} = 9.0$, whereas, the lower frequency estimate (based on the normal modes or free oscillations of the Earth) was $M_w = 9.3$ (Stein and Okal, 2005).

The published data for the M_w–M_L relationships (Table 3.6 in (Bormann et al., 2013)) includes the variants of linear (with different b-values) and nonlinear relationships; here, in the case of a broad range of magnitudes (2.5–7.5), this relationship is almost always nonlinear (e.g., (Hanks and Boore, 1984; Gusev and Melnikova, 1992)). However, it turned out that in the interval $M_w = 3$–6, which is studied in our work, the simplest variant of this relationship—linear with $b = 1$—is entirely acceptable. There is no doubt that nonlinearity will be observed on either side of this interval (beyond it), just as in the other cases with a broad range of magnitudes. Hence, extrapolation of the suggested linear relationship both upward and downward on the magnitude scale is very undesirable. The estimate of the M_w–$K_{S1,2}^{F68}$ relationship (and, thus, indirectly M_w–M_L) of (Gusev and Melnikova, 1992) should be considered as out of date.

It can also be noted that, since the energy class is by design $K_S = \log_{10} E$, where E is the seismic energy, from relationship (4b), it can be derived that $M_0 \sim E^{0.75}$. This raises the question about the dimension of the sides of this relationship since both M_0 and E have the dimension [kg m^2/s^2]. Problems of this kind are common in the cases when the exponent in the power-law scaling is not a round number. Technically, these problems are passed around through the introduction of the reference dimension values (M_0^{ref}, E^{ref}), for instance, in the following way: $(M_0/M_0^{ref}) \sim (E/E^{ref})^{0.75}$.

Although the source energy estimate $E = 10^{K_S}$ stems from the predigital era and is of limited quality, the relationship $M_0 \sim E^{0.75}$ should still be approximately valid in the interval $M_L = 3$–6. It is instructive to look at the probable causes of this relationship. It is clear that under the assumption of similarity of the sources, M_0 and E must be proportional to each other as the parameters of the same dimension. Hence, the revealed relationship testifies to the violation of similarity. It can be shown that, given the validity of the well-known Brune model (Brune, 1970), the relationship $E \sim M_0^{4/3}$ is the case at $f_c \sim M_0^{-0.222}$, where f_c is the corner frequency, whereas in the case of similarity $f_c \sim M_0^{-1/3}$. Since in Brune's model the stress drop is $\Delta\sigma \sim f_c^3 M_0$, we may assume the probable growth of $\Delta\sigma$ with magnitude for the Kamchatka earthquakes in the interval $M_w = 3$–6.

Table 4. Examples of discrepancies between regional and global estimates M_w

$M_w^{(region)} - M_w^{GCMT}$	Region	Data source
–0.12...–0.19	Greece	(Konstantinou, 2014)
–0.27	Central Asia	(Patton, 1998)
–0.1...–0.2	France	(Drouet et al., 2010)
–0.1...–0.2	Kamchatka	This work (variants see in Table 2)

CONCLUSIONS

1. For the first time for the Russian Far East, techniques for the mass determination of M_0 for the magnitude interval 3–6 are tested and the set of hundreds of regional M_w estimates is obtained.

2. The determination threshold of magnitude M_w in the part of the regional catalog within a radius of 200 km from the group of stations close to Petropavlovsk-Kamchatskii is lowered in the present work from $M_w \approx 5.0$ to $M_w \approx 3.0$.

3. The absence of noticeable deviations between the regional LF estimates (M_w^{RSMT}) and global estimates of the same kind (M_w^{GCMT}) is verified.

4. The presence of a small (about –0.1) negative bias is established in the medium-frequency M_w estimates based on the S- and coda waves compared to the LF estimates; a similar underestimation is systematically observed in the other regions.

5. For the magnitude range 3–6, a formula is recommended for converting the $K_{S1,2}^{F68}$ and M_L values of the regional catalog for the previous period into the proxy-M_w estimates of the regional earthquakes.

ACKNOWLEDGMENTS

The work was partially carried out at the Kamchatka Branch of the Geophysical Survey of the Russian Academy of Sciences with the support from the Russian Science Foundation (project no. 14-17-00621).

We are grateful to the reviewers O.V. Pavlenko and I.P. Gabsatarova and to the science editor V.B. Smirnov for their useful comments and recommendations.

REFERENCES

Abubakirov, I.R. and Gusev, A.A., Estimation of scattering properties of lithosphere of Kamchatka based on Monte-Carlo simulation of record envelope of a near earthquake, *Phys. Earth Planet. Inter.,* 1990, vol. 64, no. 1, pp. 52–67.

Aptekman, Zh.Ya., Belavina, Yu.F., Zakharova, A.I., Zobin, V.M., Kogan, S.Ya., Korchagina, O.A., Moskvina, A.G., Polikarpova, L.A., and Chepkunas, L.S., *P*-wave spectra in the problem of determining the dynamic parameters of earthquake sources. Conversion from station spectrum to source spectrum and calculation of the dynamic parameters of the source, *Vulkanol. Seismol.*, 1989, no. 2, pp. 66–79.

Boore, D.M. and Boatwright, J., Average body-wave radiation coefficients, *Bull. Seismol. Soc. Am.*, 1984, vol. 74, no. 5, pp. 1615–1621.

Boore, D.M., Simulation of ground motion using the stochastic method, *Pure Appl. Geophys.*, 2003, vol. 160, pp. 635–676.

Bormann, P., Wendt, S., and DiGiacomo, D., Seismic sources and source parameters, in *New Manual of Seismological Observatory Practice 2 (NMSOP2)*, Bormann, P., Ed., Potsdam: Deutsches GeoForschungsZentrum GFZ, 2013, pp. 1–259.

Bormann, P. and Dewey, J. W., The new IASPEI standards for determining magnitudes from digital data and their relation to classical magnitudes, in *New Manual of Seismological Observatory Practice 2 (NMSOP-2)*, Bormann, P., Ed., Potsdam: Deutsches GeoForschungsZentrum GFZ, 2014, pp. 1–44.

Brune, J.N., Tectonic stress and the spectra of seismic shear waves from earthquakes, *J. Geophys. Res.,* 1970, vol. 75, no. 26, pp. 4997–5009.

Bune, V.I., On the classification of the earthquakes by the energy of elastic waves radiated from the source, *Dokl. Akad. Nauk Tadzh. SSR*, 1955, no. 14, pp. 31–34.

Chebrov, V.N., Droznin, D.V., Kugaenko, Yu.A., Levina, V.I., Senyukov, S.L., Sergeev, V.A., Shevchenko, Yu.V., Yaschuk, V.V., The system of detailed seismological observations in Kamchatka in 2011, *Volcanol. Seismol.*, 2013, vol. 7, no. 1, pp. 16–36.

Chebrov, V.N., Kugaenko, Yu.A., Abubakirov, I.R., Droznina, S.Ya., Ivanova, E.I., Matveenko, E.A., Mitiushkina, S.V., Ototiuk, D.A., Pavlov, V.M., Raevskaia, A.A., Saltykov, V.A., Seniukov, S.L., Serafimova, Yu.K., Skorkina, A.A., Titkov, N.N., Chevrov,D.V., Zhupanovskoe earthquake of 30.01.2016 with $K_S = 15.7$, $M_w = 7.2$, $I = 6$ (Kamchatka), Vestn. KRAUNTs, *Nauki Zemle*, 2016, vol. 29, no. 1, pp. 5–16.

Drouet, S., Cotton, F., and Gueguen, P., Vs30, κ, regional attenuation and M_w from accelerograms: application to magnitude 3–5 French earthquakes, *Geophys. J. Int.*, 2010, vol. 182, no. 2, pp. 880–898.

Dziewonski, A.M. and Anderson, D.L., Preliminary reference Earth model, *Phys. Earth Planet. Inter.*, 1981, vol. 25, no. 4, pp. 297–356.

Dziewonski, A.M., Chou, T.A., and Woodhouse, J.H., Determination of earthquake source parameters from waveform data for studies of global and regional seismicity, *J. Geophys. Res.,* 1981, vol. 86, no. B4, pp. 2825–2852.

Edwards, B., Allmann, B., Fah, D., and Clinton, J., Automatic computation of moment magnitudes for small earthquakes and the scaling of local to moment magnitude, *Geophys. J. Int.*, 2010, vol. 183, no. 1, pp. 407–420.

Ekström, G., Nettles, M., and Dziewonski, A.M., The global CMT project 2004–2010: centroid-moment tensors for 13017 earthquakes, *Phys. Earth Planet. Inter.*, 2012, vol. 200, pp. 1–9.

Fedotov, S.A., *Energeticheskaya klassifikatsiya Kurilo-Kamchatskikh zemletryasenii i problema magnitud* (Energy Classification of the Kuril–Kamchatka Earthquakes and the Problem of Magnitudes), Moscow: Nauka, 1972.

Gasperini, P., Lolli, B., Vannucci, G., and Boschi, E., A comparison of moment magnitude estimates for the European–Mediterranean and Italian regions, *Geophys. J. Int.*, 2012, vol. 190, no. 3, pp. 1733–1745.

Gordeev, E.I., Gusev, A.A., Levina, V.I., Leonov, V.L., and Chebrov, V.N., Shallow earthquakes in Kamchatka Peninsula, *Vulkanol. Seismol.*, 2006, no. 3, pp. 28–38.

Guseva, E.M., Gusev, A.A., and Oskorbin, L.S., A software package for earthquake data processing: experimental application to strong motion records, *Volcanol. Seismol.*, 1991, vol. 11, no. 5, pp. 648–670.

Gusev, A.A. and Melnikova, V.N., Relationships between magnitude scales for global and Kamchatka earthquakes, *Volcanol. Seismol.*, 1992, vol. 12, no. 6, pp. 723–733.

Gusev, A.A. and Shumilina, L.S., Recurrence of Kamchatka strong earthquakes on a scale of moment magnitudes, *Izv., Phys. Solid Earth*, 2004, vol. 40, no. 3, pp. 206–215.

Gusev, A.A. and Guseva, E.M., Shear wave attenuation estimated from the spectral decay rate in the vicinity of the Petropavlovsk station, Kamchatka, *Izv., Phys. Solid Earth*, 2016a, vol. 52, no. 4, pp. 503–519.

Gusev, A.A. and Guseva, E.M., Source spectra of near Kamchatka earthquakes: recovering them from S-wave spectra, and determination of scaling for three corner frequencies, *Pure Appl. Geophys.*, 2016b, vol. 173, no. 5, pp. 1539–1557.

Hanks, T.C. and Kanamori, H., A moment magnitude scale, *J. Geophys. Res.*, 1979, vol. 84, no. B5, pp. 2348–2350.

Hanks, T.C. and Boore, D.M., Moment-magnitude relations in theory and practice, *J. Geophys. Res.*, 1984, vol. 89, no. B7, pp. 6229–6235.

Kanamori, H., The energy release in great earthquakes, *J. Geophys. Res.*, 1977, vol. 82, no. 20, pp. 2981–2987.

Kennett, B.L.N., Engdahl, E.R., and Buland, R., Constraints on seismic velocities in the Earth from traveltimes, *Geophys. J. Int.*, 1995, vol. 122, no. 1, pp. 108–124.

Konstantinou, K.I., Moment magnitude-rupture area scaling and stress-drop variations for earthquakes in the Mediterranean region, *Bull. Seismol. Soc. Am.*, 2014, vol. 104, no. 5, pp. 2378–2386.

Maeda, T. and Sasatani, T., Two-layer Qs structure of the slab near the southern Kurile trench, *Earth, Planets Space*, 2006, vol. 58, no. 5, pp. 543–553.

Patton, H.J., Bias in the centroid moment tensor for central Asian earthquakes: evidence from regional surface wave data, *J. Geophys. Res.*, 1998, vol. 103, no. B11, pp. 26963–26974.

Pavlenko, O.V., Simulation of ground motion from strong earthquakes of Kamchatka region (1992–1993) at rock and soil sites, *Pure Appl. Geophys.*, 2013, vol. 170, no. 4, pp. 571–595.

Pavlov, V.M. and Abubakirov, I.R., Algorithm for calculation of seismic moment tensor of strong earthquakes using regional broadband seismograms of body waves, *Vestnik KRAUNTs. Nauki Zemle*, 2012, vol. 20, no. 2, pp. 149–158.

Pavlov, V.M., Algorithm for calculating synthetic seismograms in a layered half-space with application of matrix impedance, *Izv., Phys. Solid Earth*, 2013, vol. 49, no. 1, pp. 24–33.

Petukhin, A.G. and Gusev, A.A., The duration-distance relationship and average envelope shapes of small Kamchatka earthquakes, *Pure Appl. Geophys.*, 2003, vol. 160, no. 9, pp. 1717–1743.

Rautian, T.G., Energy of earthquakes, in *Metody detal'nogo izucheniya seismichnosti. Trudy IFZ AN SSSR* (Methods for Detailed Studying the Earthquakes. Proc. Schmidt Institute of Physics of the Earth of the USSR Academy of Sciences), vol. 176, 1960, no. 9, pp. 75–114.

Rautian, T.G. and Khalturin, V.I., The use of the coda for determination of the earthquake source spectrum, *Bull. Seismol. Soc. Am.*, 1978, vol. 68, no. 4, pp. 923–948.

Rautian, T.G., Khalturin, V.I., Zakirov, M.S., Zemtsova, A.G., Proskurin, A.P., Pustovitenko, B.G., Pustovitenko, A.N., Sinel'nikova, L.G., Filina, A.G., and Shengeliya, I.S., *Eksperimental'nye issledovaniya seismicheskoi kody* (Experimental Studies in Seismic Coda), Moscow: Nauka, 1981.

Seismological Data Information System (SDIS) of the Kamchatka Branch of Geophysical Survey of Russian Academy of Science. http://www.emsd.ru/sdis (Cited January 16, 2017).

Skorkina, A.A. and Gusev, A.A., Determination of corner frequencies of source spectra for subduction earthquakes in Avacha Gulf (Kamchatka), *Rus. Geol. Geophys.*, 2017, vol. 58, no. 7, pp. 844–854.

Stein, S. and Okal, E.A., Seismology: speed and size of the Sumatra earthquake, *Nature*, 2005, vol. 434, no. 7033, pp. 581–582.

Tsai, V.C., Nettles, M., Ekstrom, G., and Dziewonski, A.M., Multiple CMT source analysis of the 2004 Sumatra earthquake, *Geophys. Res. Lett.*, 2005, vol. 32, no. 17, p. L17304.

Translated by M. Nazarenko